

# Growth dynamics of bubbles on a pore-patterned surface under reduced pressure

Cite as: Phys. Fluids 31, 097101 (2019); <https://doi.org/10.1063/1.5120362>

Submitted: 17 July 2019 . Accepted: 14 August 2019 . Published Online: 03 September 2019

Jiayan Li (李佳燕), Jiangen Zheng (郑建良), Yingzhou Huang (黄映洲) , and Guo Chen (陈果) 



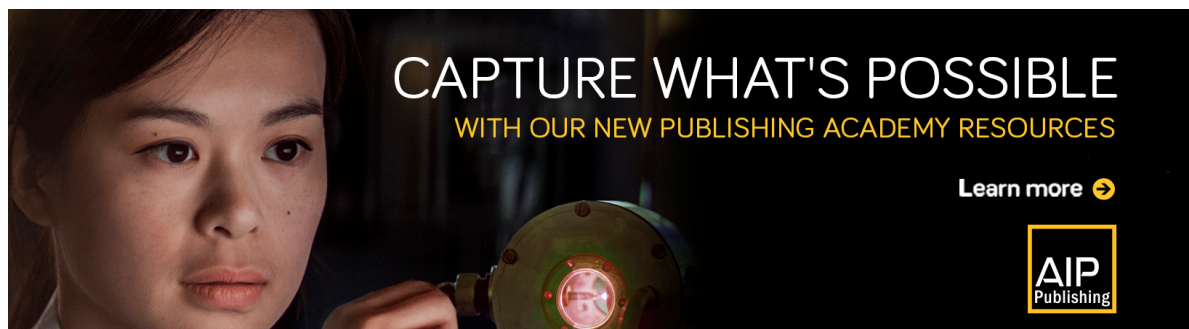
View Online




Export Citation





CrossMark



CAPTURE WHAT'S POSSIBLE  
WITH OUR NEW PUBLISHING ACADEMY RESOURCES

Learn more 



# Growth dynamics of bubbles on a pore-patterned surface under reduced pressure

Cite as: *Phys. Fluids* **31**, 097101 (2019); doi: [10.1063/1.5120362](https://doi.org/10.1063/1.5120362)

Submitted: 17 July 2019 • Accepted: 14 August 2019 •

Published Online: 3 September 2019



View Online



Export Citation



CrossMark

Jiayan Li (李佳燕),<sup>a)</sup> Jiangen Zheng (郑建良),<sup>a)</sup> Yingzhou Huang (黄映洲),<sup>b)</sup>  and Guo Chen (陈果)<sup>b)</sup> 

## AFFILIATIONS

Chongqing Key Laboratory of Soft Condensed Matter Physics and Smart Materials, College of Physics, Chongqing University, Chongqing 400044, China

<sup>a)</sup> **Contributions:** J. Li and J. Zheng contributed equally to this work.

<sup>b)</sup> **Authors to whom correspondence should be addressed:** [yzhuang@cqu.edu.cn](mailto:yzhuang@cqu.edu.cn) and [wezer@cqu.edu.cn](mailto:wezer@cqu.edu.cn)

## ABSTRACT

The growth dynamics of bubbles has been extensively studied for several decades. However, a thorough understanding of the morphological evolution of bubbles on pore-patterned surfaces through the coalescence of adjacent bubbles induced by expansion is still lacking. This study aims to quantitatively investigate the coalescence of adjacent bubbles in drops on customized microscale pore-patterned surfaces from the bottom view under different atmospheric pressures. The results demonstrate that the coalescence status and the size of bubbles can be controlled by adjusting the atmospheric pressure and are also in good agreement with the theoretical analysis results. This work provides insight into the underlying physics of growing bubbles on a pore-patterned surface; this is important for research on gas–fluid–solid interfacial slips and surface drag reduction.

Published under license by AIP Publishing. <https://doi.org/10.1063/1.5120362>

## INTRODUCTION

Surfaces with pore-patterned structures have broad applications ranging from antifouling<sup>1,2</sup> and cavitation control<sup>3</sup> to drag reduction<sup>4–8</sup> and heat transfer.<sup>9–11</sup> The key to achieving these functions is to entrap a large volume of gas in the cavities of these structures to form gas bubble clusters. Gas entrapped in these structures plays significant roles in realizing the applications mentioned above, and their morphologies could markedly affect physical effects such as flow slip,<sup>12</sup> droplet adhesion,<sup>13</sup> and cavitation.<sup>3,14,15</sup> Therefore, better functional performance and quality of structured surfaces based on gas cavities require a profound understanding of the morphological evolution of the gas bubble.

Currently, there are several methods for studying the morphological evolution of a bubble, such as depressurization,<sup>16–18</sup> solvent exchange,<sup>19,20</sup> gas diffusion,<sup>21–23</sup> and vibration.<sup>3,24</sup> For example, the location, number density, and size of bubbles influenced by the distance between the seeding air pockets on an array can be studied by using solvent exchange.<sup>20</sup> Among the mentioned methods, the response of gas entrapped in a pore-patterned surface to depressurization is one of the most widely used methods. In recent years,

much work has been focused on the morphology of the gas bubble. On the one hand, the cavity morphological change under reduced liquid pressure can be divided into five stages: pinned recession, depinned recession, a Cassie–Baxter state, expansion, and coalescence.<sup>16</sup> Furthermore, the air diffusion induced the bubble evolution process under reduced pressure has been researched, and the morphological behavior of a collection of neighboring bubbles comprises four typical evolution phases, namely, growth, coalescence, shrinkage, and splitting.<sup>25</sup> Moreover, the underlying mechanisms of the morphology evolution of a liquid–gas interface on submerged solid structured surfaces under both quiescent and flow conditions have been systematically summarized.<sup>26–28</sup> On the other hand, the morphological instability of the bubble under arbitrary amplitude distortions has been studied based on the comparison of entropy productions for a distorted and undistorted surface and using the maximum entropy production principle.<sup>29</sup> The transition in interfacial instability behavior of bubble occurs with an increase in superheat; the bubble release being periodic both in space and time has also been investigated.<sup>30</sup>

However, thorough understanding of the morphological evolution of small bubbles on pore-patterned surfaces through a collection of adjacent bubbles induced by expansion is still lacking.

Moreover, as bubbles in a real environment or industry often appear on rough surfaces, the study of the morphological evolution of bubbles in complex environment has general and practical significance. The goal of this study is to investigate the air expansion induced bubble evolution process and comprehensively determine the morphological behavior of a collection of neighboring bubbles on submerged pore-patterned structures under reduced atmospheric pressure using microscopy from the bottom. Three typical evolution stages, referred to as the delayed stage, coalescence and expansion stage, and self-adjusting stage, are captured *in situ*. Then, the evolution of the area ratio  $S$  with time is analyzed under different atmospheric pressures. Finally, the relationships between the delay time  $t_d$  and the area ratio  $S_e$  at the final equilibrium state and the atmosphere pressure difference are discussed using the experimental results and theoretical analyses.

## EXPERIMENTAL SECTION

The morphological changes of small bubbles on pore-patterned surfaces were studied through a collection of adjacent bubbles experiments performed in a transparent glass chamber with controlled atmospheric pressures; the schematic of the experimental system is shown in Fig. 1(a). The glass chamber had an inner size of  $60 \times 60 \times 80 \text{ mm}^3$ , and a pore-patterned polydimethylsiloxane (PDMS) substrate was placed at the bottom of the chamber. Then, the glass chamber was mounted on a microscope (OLYMPUS IX73, Japan) equipped with a  $10\times$  objective ( $NA = 0.3$ ) and Charge Coupled Device (CCD, Olympus DP73, Japan). The samples with microscale pore-patterned structures were obtained by reverse-mold with PDMS through a micropillar structure template, where the mold with the pillar pattern was fabricated by standard ultraviolet (UV) photolithography (URE-2000/35, China) and dry-etching on a clean silicon wafer. The pores on these substrates had

the same height  $H$  ( $21 \mu\text{m}$ ) and diameters  $D$  ( $55 \mu\text{m}$ ), but the spaces between them had different sizes  $L$  ( $45, 95, \text{ and } 145 \mu\text{m}$ ), as shown in Fig. 1(b).

The pressure of the chamber,  $P_{\text{chamber}}$ , was controlled by a vacuum control system that was mainly composed of a solenoid valve (Burkert DS2705, Germany), solenoid valve controller (Burkert DS8605, Germany), and pressure transmitter (PRC-905, China), and the absolute pressure inside the chamber ( $p_{\text{chamber},1}$ ) could be varied between 10 and 101 kPa with a precision of 1% through the outlet of the chamber, as shown in Fig. 1(a). In this paper, all the values of pressure are the relative pressure values. The pressure difference is denoted by  $\Delta p = p_{\text{chamber},1} - p_{\text{chamber},0}$ , where  $P_{\text{chamber},0} = 101 \text{ kPa}$  is the initial atmospheric pressure. All the experiments were carried out at a constant room temperature of  $22 \pm 1^\circ\text{C}$  and constant humidity of  $60\% \pm 5\%$ . Before the experiments commenced,  $15 \mu\text{l}$  of milli-Q deionized water was carefully introduced as a droplet onto the substrate by pipette (Eppendorf research plus,  $2\text{--}20 \mu\text{l}$ , Germany) without causing any visible bubbles to appear outside the holes. The corresponding evolution of the bubbles was recorded by CCD (Olympus DP73, Japan) at a frame rate of 15 fps when the atmospheric pressure in the chamber began to decrease. All experiments with identical conditions were repeated at least five times to make sure that our results are generally valid. Then, we use Matlab software to process the obtained experimental videos. First, the gas region and water region were separated through image binary processing. Then, the number of pixels in the gas region and that of the entire field of view were counted to calculate the area ratio.

## RESULTS AND DISCUSSION

A change in the atmospheric pressure can significantly alter the expansion ratio of gas and the contact area between a gas and a substrate. First, by comparing the bottom-view images, we found that

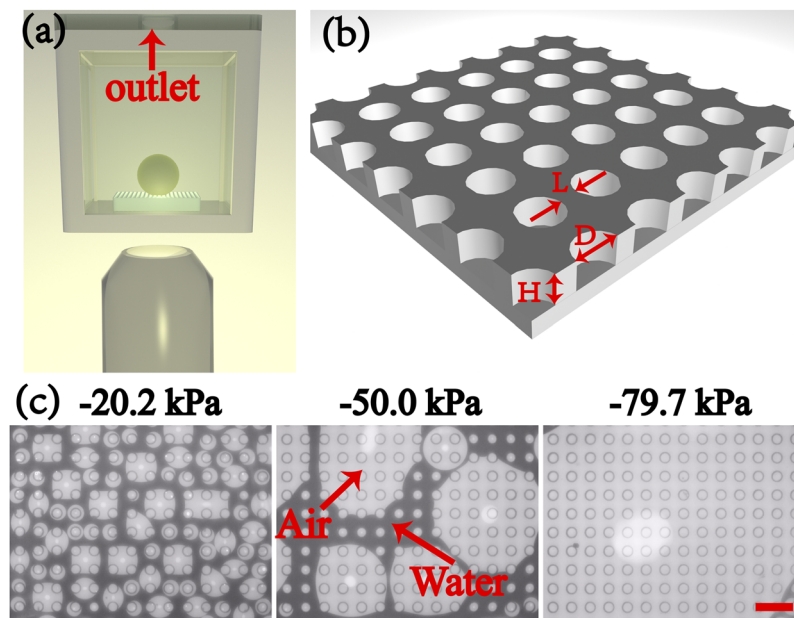


**FIG. 1.** (a) Schematics of the experiment setup for the *in situ* observation of bubble growth from the bottom. A drop is placed on a pore-patterned polydimethylsiloxane (PDMS) substrate inside a transparent vacuum chamber. (b) Three-dimensional schematic of a microstructured surface with cylindrical pores of diameter  $D$  and depth  $H$ ; the space between two neighboring holes is  $L$ . (c) Bottom-view images of the equilibrium morphology at the substrate interface after the atmospheric pressure was reduced to  $\Delta P = -20.2 \text{ kPa}$ ,  $-50.0 \text{ kPa}$ , and  $-79.7 \text{ kPa}$ , where the white area is air and the black area is water. The parameters of the pore-patterned structure of the substrate are  $D = 55 \mu\text{m}$ ,  $L = 45 \mu\text{m}$ , and  $H = 21 \mu\text{m}$ . The scale bar is  $200 \mu\text{m}$ .

the surface morphologies of the bubbles inside the drop vary under different atmospheric pressures. The pressure differences were  $\Delta P = -20.2$  kPa,  $-50.0$  kPa, and  $-79.7$  kPa, as shown in Fig. 1(c). The white area and the black area are air and water, respectively. The area of the gas zone and the entire field of view are defined as  $S_g$  and  $S_{\text{view}}$ , respectively. We can conclude that the larger the area of air in the field of view, the larger the atmospheric pressure difference. Then, we investigated the features of the correspondingly expanding bubbles in response to a rapid reduction in the atmospheric pressure from 0 kPa to  $-56.0$  kPa, by comparing the area ratio ( $S = S_g/S_{\text{view}}$ ) of the gas area to the entire field of view at different times, one typical result is shown in Fig. 2(a). When the pressure of the chamber was reduced from 0 kPa to  $-56$  kPa, the entrapped air expanded gradually because of the reduced pressure.

The growing process can be divided into three stages according to the evolution of  $S$ : (I) Delayed stage, where the value of  $S$  is constant.  $t_0 = 0$  s and  $t_1 = 2.3$  s are the initial times at which the atmosphere pressure begins to decrease, and the area ratio  $S$  begins to increase, respectively. Initially, the pressure reduction occurs, while the water droplet on the pore-patterned substrate is in a Cassie-Baxter state, that is, the liquid has a protruding gas-liquid interface (the protruding meniscus) relative to the surface of the pore-patterned substrate, as shown in inset I in Fig. 2. Then, the protruding meniscus pins in the top corner undergo growth upward, and the contact angle decreases until it reaches the receding angle  $\theta_r$  and the highest point of the meniscus moves to  $h$ , as shown in inset I in Fig. 2(a). Therefore, we defined the delay time as  $t_d = t_1 - t_0$ ; (II) expansion and coalescence stage, where the receding angle on the pore-patterned surface is reached and the protruding meniscus depins, forming a bubbly cap. Once the small bubbles expand until the adjacent bubbles touch each other, coalescing occurs to form a bubble with a greater size as the atmosphere pressure further decreases. Two, three, or four small neighboring bubbles coalesce

to achieve dynamic equilibrium as a result of the reduced atmospheric pressure, as shown in the image taken at time  $t_2 = 5$  s on the right side of Fig. 2(b); therefore, the value of  $S$  grows rapidly during this stage; (III) self-adjusting stage, where the bubbles continue to expand under the low atmospheric pressure after the coalescence, and their shapes are adjusted so that they gradually achieve a stable equilibrium state, in which the total free energy is minimized. The value of  $S$  fluctuates continuously, but the change is very small. In this stage, the fluctuation of  $S$  is mainly caused by the occasional coalescence of large bubbles, which can also be seen in the bottom-view images taken at  $t_3$  and  $t_4$ . Paying attention to the red dotted line area in images taken at  $t_3$  and  $t_4$ , one can see that at time  $t_3 = 32.0$  s, there is still a thin liquid film separating the two bubbles in the area, but at time  $t_4 = 32.6$  s, the liquid film breaks and the two big bubbles merge into one larger bubble. At this time, the gas area is reduced, which is reflected in a sudden decrease in  $S$ , and then each bubble continues to expand slowly. This process is repeated several times until the equilibrium state is achieved at  $t_5 = 75.0$  s, as shown in Fig. 2(b).

Then, we investigated the evolution of the area ratio  $S$  with time in response to different atmospheric pressures [Fig. 3(a)]. Comparing the changes of  $S$  with time in response to four different pressure differences, we find that there is a delayed stage in all cases, and the delay time decreases with a decrease in atmospheric pressure  $\Delta P$ . When the pressure difference is  $\Delta P = -79.7$  kPa, the value of  $S$  does not change at first. Then, the small bubbles coalesce, expand, and self-adjust rapidly to form the final large bubbles within 60 s. At the end of this process, the area ratio  $S$ , which is close to 1, is the largest of the four cases, indicating that the entire field of view is almost occupied by one big bubble. The change in  $S$  is more complicated in the expansion and coalescence stage caused by the large reduced atmosphere pressure  $\Delta P$ . For example, the value of  $S$  jumped between  $t_1$  and  $t_2$ , as shown in Fig. 3(a). Comparing the changes in the red dotted circle of the images at two moments,

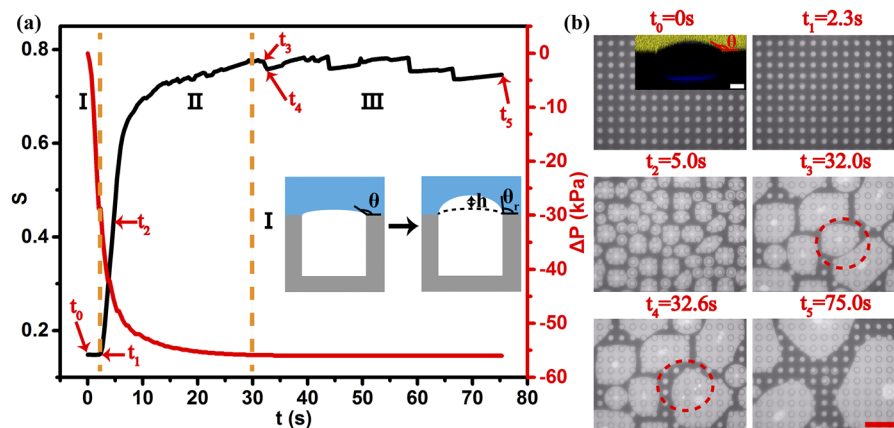


**FIG. 2.** (a) Variation in the area ratio  $S$  and the atmospheric pressure difference  $\Delta P$  during the growth of the bubbles in response to a rapid reduction in the atmospheric pressure from 0 kPa to  $-56.0$  kPa. The black line represents the experimental results of the area ratio  $S$ , while the red line represents the atmospheric pressure. Inset I illustrates the state of the gas-liquid interface and cavity morphology of the bubble growth at stage I.  $\theta = 135^\circ$  and  $\theta_r = 94^\circ$  are the initial contact angle and receding contact angle, respectively.  $h$  is the movement distance of the highest point of the protruding meniscus at stage I. (b) Bottom-view images showing bubble expansion and coalescence evolution with time (the scale bar is 300  $\mu\text{m}$ ). The parameters of the pore-patterned structure of the substrate are  $D = 55$   $\mu\text{m}$ ,  $L = 45$   $\mu\text{m}$ , and  $H = 21$   $\mu\text{m}$ . The inset is a 3-D reconstructed confocal image showing the Cassie-Baxter state of the droplet on the pore-patterned substrate. Scale bar: 10  $\mu\text{m}$ .

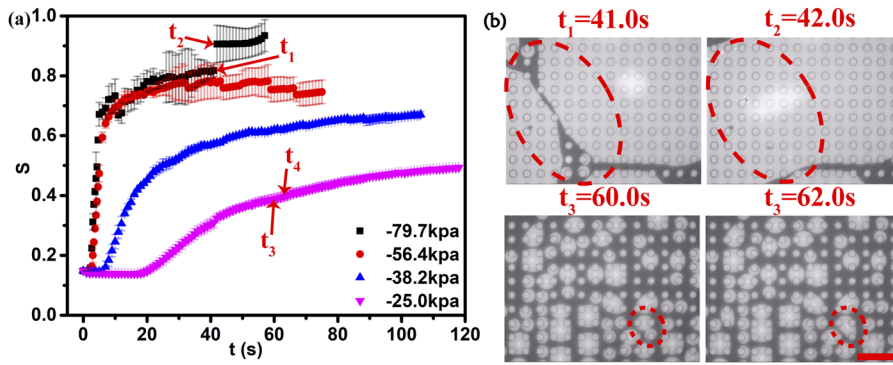


**FIG. 3.** (a) Revolution of the area ratio  $S$  with time in response to different atmospheric pressure differences. The parameters of the pore-patterned structure of the substrate are  $D = 55 \mu\text{m}$ ,  $L = 45 \mu\text{m}$ , and  $H = 21 \mu\text{m}$ . (b) Bottom-view images of bubbles at the four different moments we focused on. The scale bar is  $300 \mu\text{m}$ .

$t_1 = 41.0 \text{ s}$  and  $t_2 = 42.0 \text{ s}$ , before and after the jump in the value of  $S$ , we find that the jump in the value of  $S$  is due to the coalescence of neighboring large bubbles.

Therefore, in the case of large depressurization, there are many large bubbles on the pore-patterned surface at the self-adjust stage, and the change in the  $S$  value shows many large jumps, all of which are derived from the coalescence of large bubbles. As a contrast, the value of  $S$  increases slowly over time in the second and third stages through the expansion and coalescence of small bubbles when the pressure difference is  $\Delta P = 25.0 \text{ kPa}$ . The entire process takes a longer time. Why does the value of  $S$  not jump significantly at this reduced atmosphere pressure  $\Delta P$ ? By comparing the images taken at  $t_3 = 60.0 \text{ s}$  and  $t_4 = 62.0 \text{ s}$  in Fig. 3(b), we find that there are scattered small bubbles in the field of view, and the value of  $S$  increases only because of the coalescence of individual bubbles, as shown in the red dotted circle, so the change is relatively small. Finally, we come to the conclusion that the magnitude of ambient pressure reduced the effects of the variation in area ratio  $S$ , such as delay time, change rate, and final value.

Because the area ratio remains constant in response to different atmospheric pressure reductions for some substrates, we focus on the delay time in this section. Figure 4(a) shows the variation in the delay time  $t_d$  in response to different pressure reductions for six different substrates.

In all cases, the longest delay time we observed was only about 2 min, which is much smaller than the time scale of gas diffusion (tens of minutes<sup>31</sup>). Therefore, only the expansion of gas trapped in the holes was considered in this study. The depth of the holes for all the substrates is  $H = 21 \mu\text{m}$ . D55L45, D55L95, D55L145, D23L37, D29L19, and D84L50 in the figure represent the parameters of the pore-patterned structures of the substrates, where the diameter  $D$  is  $55 \mu\text{m}$ ,  $23 \mu\text{m}$ ,  $29 \mu\text{m}$ , and  $84 \mu\text{m}$ , and the hole spacing  $L$  is  $45 \mu\text{m}$ ,  $95 \mu\text{m}$ ,  $145 \mu\text{m}$ ,  $37 \mu\text{m}$ ,  $19 \mu\text{m}$ , and  $50 \mu\text{m}$ , respectively. Comparing the delay time of each substrate at different atmosphere pressure differences as shown in Fig. 4(a), we find that, with an increase in the atmospheric pressure difference  $\Delta P$ , the growth time increases, which means that the time taken to complete the growth of the gas-liquid interface at the hole increases. The growth trend of the delay time for different substrates is consistent. The delay time of the all substrates is about 2 s when the atmospheric pressure difference is small ( $-40 \text{ kPa}$  or less), but it is more than 2 s and constantly increasing when the atmosphere pressure difference is large ( $-40 \text{ kPa}$  to  $-10 \text{ kPa}$ ). However, the relationship between  $t_d$  and  $\Delta P$  still needs further exploration.

During the delay time, the growth of the gas-liquid interface (the protruding meniscus) on the hole is considered to be described by the Rayleigh-Plesset model.<sup>32</sup> First, it is necessary to consider the gravitational force of the liquid column above the hole and the driving force of the protruding meniscus caused by the atmosphere pressure difference. The gravitational force of the liquid column above the hole is  $F_g = \rho \pi D^2 h^* g / 4$ , where  $\rho = 1.01 \times 10^3 \text{ kg/m}^3$  is the density of water,  $g = 9.8 \text{ m/s}^2$  is the acceleration of gravity,  $h^* \approx 3 \times 10^{-3} \text{ m}$  is the height of the droplet on the surface of the hole, and  $D = 55 \mu\text{m}$  is the characteristic size, which is equal to the diameter of the hole. The driving force of the gas-liquid interface caused by the atmosphere pressure difference is  $F_d = |\Delta P| \times D^2 \approx 2.4 \times 10^{-8} \text{ kg m/s}^2$ . Then,  $F_d / F_g \approx 3.42 \times 10^3 \gg 1$ , which reveals that  $F_g$  can be negligible compared with  $F_d$  in our experiments. Then, the Rayleigh-Plesset

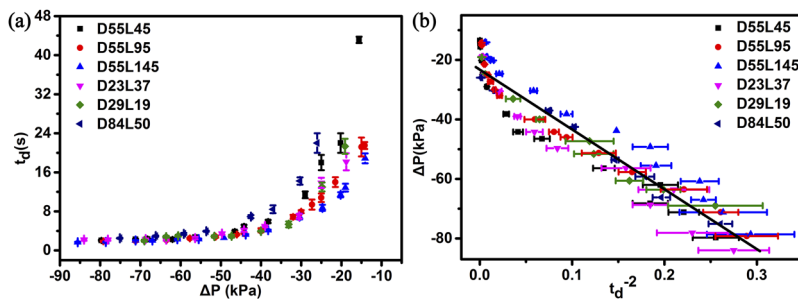


**FIG. 4.** (a) Variation in the delay time  $t_d$  in response to different pressure reductions for different substrates. (b) Plot of  $\Delta P$  as a function of  $t_d^{-2}$  for different substrates.

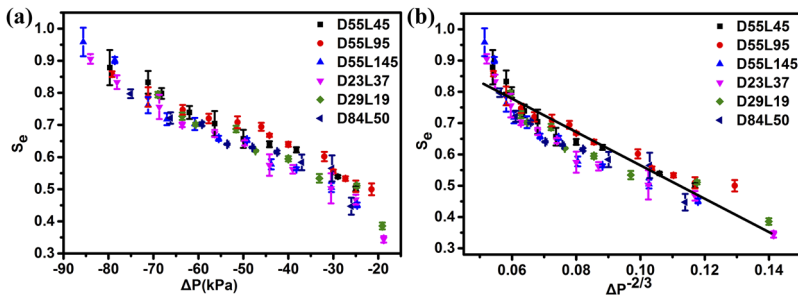


**FIG. 5.** (a) Variation in the area ratio  $S_e$  at the final equilibrium state in response to different atmospheric pressure differences  $\Delta P$  for different substrates. (b) The area ratio  $S_e$  as a function of  $\Delta P^{-2/3}$  for different substrates. The black solid line is drawn as a guide for the eye.

equation in our experiment can be written as follows:

$$\rho \frac{dv}{dt} + \frac{3\rho v^2}{2D} = \frac{|\Delta P|}{D} - \frac{\eta v}{D^2} - \frac{2\gamma}{D^2}, \quad (1)$$

where  $\eta$  and  $\gamma$  are the viscosity and surface tension of water, respectively. Plugging in the typical values,  $\Delta P = -79.7$  kPa,  $D = 55$   $\mu\text{m}$ ,  $v = 10$   $\mu\text{m/s}$ ,  $\rho = 1 \times 10^3$   $\text{kg/m}^3$ ,  $\eta = 1 \times 10^{-3}$  Pa s, and  $\gamma = 72 \times 10^{-3}$  N/m, we obtain  $\frac{|\Delta P|}{D} / \frac{3\rho v^2}{2D} \cong 5.28 \times 10^{15} \gg 1$ ,  $\frac{|\Delta P|}{D} / \frac{\eta v}{D^2} \cong 4.35 \times 10^8 \gg 1$ , and  $\frac{|\Delta P|}{D} / \frac{2\gamma}{D^2} \cong 30.25 \gg 1$ . These results reveal that  $\frac{3\rho v^2}{2D}$ ,  $\frac{\eta v}{D^2}$ , and  $\frac{2\gamma}{D^2}$  can be negligible compared with  $\frac{|\Delta P|}{D}$  in our experiments.

Finally, based on the above analysis, we get

$$\rho \frac{dv}{dt} = \frac{|\Delta P|}{D}. \quad (2)$$

Further integration of Eq. (2) gives

$$h = \frac{|\Delta P|}{2\rho D} t_d^2. \quad (3)$$

As  $h$ ,  $\rho$ , and  $D$  are constants in our experiments, we get  $|\Delta P| \propto t_d^{-2}$ , that is,

$$\Delta P \propto t_d^{-2}. \quad (4)$$

Figure 4(b) shows the proportional relationship between  $\Delta P$  and  $t_d^{-2}$ , which is consistent with our calculation.

The area ratios  $S_e$  at the final equilibrium state at different atmospheric pressure differences for different parameters of pore-patterned structures of substrates are shown in Fig. 5(a). We find that the area ratio  $S_e$  in the final equilibrium state decreases with an increase in the atmospheric pressure difference  $\Delta P$  for different substrates. Moreover, the values of  $S_e$  for the different substrates are almost the same for the same pressure difference, which indicates that the area ratio of the final stable state is only related to the atmosphere pressure difference. It is not related to parameters of the pore-patterned structure of the substrates. We can now discuss the relationship between  $S_e$  and  $\Delta P$ . The thermal Peclet number in our experiment is defined as  $Pe = \frac{Dv}{\alpha} = \frac{Dv\rho_{\text{air}}C_p}{k}$ , where  $v$  is the flow velocity of air,  $\rho_{\text{air}}$  is the density of air,  $C_p$  is the heat capacity of air, and  $k$  is the thermal conductivity. Plugging in the typical values,  $D = 55$   $\mu\text{m}$ ,  $v = 10$   $\mu\text{m/s}$ ,  $\rho_{\text{air}} = 1.2$   $\text{kg/m}^3$ ,  $k = 0.026$  W/(mK), and  $C_p = 1 \times 10^3$  J/(kg K), we obtain  $Pe = 2 \times 10^{-5} \ll 1$ , suggesting that the heat transportation is dominated by diffusion. Suppose there is a temperature difference  $\Delta T$ . The thermal gradient becomes  $\Delta T/D$ , and the heat flux per unit time is  $dQ/dt \cong k\Delta T/D$ . This heat flux will bring the system back to equilibrium during the time scale

$\tau \cong C_p\rho_{\text{air}}V_{\text{air}}\Delta T/(dQ/dt) \cong C_p\rho_{\text{air}}D^2/k$ . The typical value for  $\tau$  is 100  $\mu\text{s}$ , which is far less than the typical expansion time (several seconds to tens of seconds). Therefore, the trapped air reaches thermal equilibrium very rapidly and undergoes an isothermal expansion process in our experiments. We have  $PV = C$  according to the ideal gas state equation, where  $C$  is a constant. Then, we can obtain  $P_0V_0 = (P_0 + \Delta P)V_e$ , where  $V_0$  and  $V_e$  are the gas volumes in the field of view at the initial time and the end time, respectively. Therefore, we can obtain  $\Delta P \propto V_e^{-1}$ . Because the morphologies of the bubbles at the final time are different, we simplify the gas in the field of view into a hemispheric bubble cap with a contact area  $S_e$ . As a result, we have  $\Delta P \propto V_e^{-1} \propto S_e^{-3/2}$ , that is  $S_e \propto \Delta P^{-2/3}$ , as shown in Fig. 5(b).

## CONCLUSIONS

In summary, we systematically investigated the morphological behavior of a collection of neighboring bubbles on submerged microscale pore-patterned structures using microscopy from the bottom. The atmosphere pressure difference varies within the range from  $-10$  kPa to  $-80$  kPa, and the bubble size is at the scale of hundred-micron in our experiments. First, the growing process was divided into three typical evolution stages according to the evolution of the area ratio  $S$ , namely, delayed stage, coalescence and expansion stage, and self-adjusting stage. Second, we found that the growth rate, smoothness, and the value at the final equilibrium state of the area ratio  $S$  were affected by the atmospheric pressure difference  $\Delta P$ . Furthermore, the delay time  $t_d$  increased with an increase in the atmospheric pressure difference and the atmospheric pressure difference was proportional to  $t_d^{-2}$  for patterned surfaces with different structure parameters. Finally, the area ratio  $S_e$  at the final equilibrium state decreased with an increase in the atmosphere pressure difference  $\Delta P$  and was proportional to  $\Delta P^{-2/3}$  for patterned surfaces with different structure parameters. This study offers insight into the area ratio variation of growing bubbles on a pore-patterned surface, which is important for studies on gas–fluid–solid interfacial slip and the drag reduction on the surface.

## ACKNOWLEDGMENTS

This work was supported by the National Natural Science Foundation of China through Grant Nos. 11604030, 11674043 and 11974067, by the Fundamental Research Funds for the Central Universities (Project Nos. 2018CDJDWL0011 and 2019CDY-GYB017), and by the Natural Science Foundation Project of CQ CSTC (cstc2019cyj-msxmX0145).

There are no conflicts of interest to declare.

## REFERENCES

- <sup>1</sup>Z. Guo and W. Liu, "Biomimic from the superhydrophobic plant leaves in nature: Binary structure and unitary structure," *Plant Sci.* **172**, 1103 (2007).
- <sup>2</sup>W. M. Katrina, W. A. Jolanta, X. P. Qu, F. J. Liu, W. S. Gregory, and C.-H. Chen, "Self-cleaning of superhydrophobic surfaces by self-propelled jumping condensate," *P. Natl. Acad. Sci. U. S. A.* **110**, 7992 (2013).
- <sup>3</sup>B. Nicolas, A. Manish, O. Claus-Dieter, and L. Detlef, "Controlled multibubble surface cavitation," *Phys. Rev. Lett.* **96**, 224501 (2006).
- <sup>4</sup>J. P. Rothstein, "Slip on superhydrophobic surfaces," *Annu. Rev. Fluid Mech.* **42**, 89 (2010).
- <sup>5</sup>S. L. Ceccio, "Friction drag reduction of external flows with bubble and gas injection," *Annu. Rev. Fluid Mech.* **42**, 183 (2009).
- <sup>6</sup>D. Saranadhi, D. Chen, J. A. Kleingartner, S. Srinivasan, R. E. Cohen, and G. H. McKinley, "Sustained drag reduction in a turbulent flow using a low-temperature Leidenfrost surface," *Sci. Adv.* **2**, e1600686 (2016).
- <sup>7</sup>S. J. Qin, C. Ning, Y. Yan, J. T. Liu, and D. Z. Wu, "Stream-wise distribution of skin-friction drag reduction on a flat plate with bubble injection," *Phys. Fluids* **29**, 037103 (2017).
- <sup>8</sup>C. M. J. Tay, B. C. Khoo, and Y. T. Chew, "Mechanics of drag reduction by shallow dimples in channel flow," *Phys. Fluids* **27**, 035109 (2015).
- <sup>9</sup>H. J. Cho, D. J. Preston, Y. Zhu, and E. N. Wang, "Nanoengineered materials for liquid-vapour phase-change heat transfer," *Nat. Rev. Mater.* **2**, 016092 (2016).
- <sup>10</sup>T. Tran, H. J. J. Staat, A. Susarrey-Arce, T. C. Foertsch, A. V. Houselt, J. G. E. G. Han, A. Prosperetti, D. Lohse, and S. Chao, "Droplet impact on superheated micro-structured surfaces," *Soft Matter* **9**, 3272 (2013).
- <sup>11</sup>A. V. Boiko, A. V. Dovgal, and A. M. Sorokin, "Modification of flow perturbations in a laminar separation bubble by heat transfer," *Phys. Fluids* **29**, 024103 (2017).
- <sup>12</sup>I. U. Vakarelski, N. A. Patankar, J. O. Marston, D. Y. C. Chan, and S. T. Thoroddsen, "Stabilization of Leidenfrost vapour layer by textured superhydrophobic surfaces," *Nature* **489**, 274 (2012).
- <sup>13</sup>K. Liu and J. Lei, "Bio-inspired self-cleaning surfaces," *Annu. Rev. Mater. Res.* **42**, 231 (2012).
- <sup>14</sup>M. A. Maiga, O. Coutier-Delgosha, and D. Buisine, "A new cavitation model based on bubble-bubble interactions," *Phys. Fluids* **30**, 123301 (2018).
- <sup>15</sup>M. A. Maiga, O. Coutier-Delgosha, and D. Buisine, "Analysis of sheet cavitation with bubble/bubble interaction models," *Phys. Fluids* **31**, 073302 (2019).
- <sup>16</sup>Y. H. Xue, P. Y. Lv, L. Ying, Y. P. Shi, and H. L. Duan, "Morphology of gas cavities on patterned hydrophobic surfaces under reduced pressure," *Phys. Fluids* **27**, 092003 (2015).
- <sup>17</sup>J. Li, H. S. Chen, W. Z. Zhou, B. Wu, S. D. Stoyanov, and E. G. Pelan, "Growth of bubbles on a solid surface in response to a pressure reduction," *Langmuir* **30**, 4223 (2014).
- <sup>18</sup>V. Tuukka, J. T. Korhonen, S. Lauri, J. Ville, B. Chris, F. Kristian, F. Sami, A. Piers, I. Olli, and R. H. A. Ras, "Reversible switching between superhydrophobic states on a hierarchically structured surface," *Proc. Natl. Acad. Sci. U. S. A.* **109**, 10210 (2012).
- <sup>19</sup>S. H. Peng, V. Spandan, R. Verzicco, D. Lohse, and X. H. Zhang, "Growth dynamics of microbubbles on microcavity arrays by solvent exchange: Experiments and numerical simulations," *J. Colloid Interface Sci.* **532**, 103 (2015).
- <sup>20</sup>S. H. Peng, T. L. Mega, and X. H. Zhang, "Collective effects in microbubble growth by solvent exchange," *Langmuir* **32**, 11265 (2016).
- <sup>21</sup>P. Y. Lv, Y. H. Xue, Y. P. Shi, H. Lin, and H. L. Duan, "Metastable states and wetting transition of submerged superhydrophobic structures," *Phys. Rev. Lett.* **112**, 196101 (2014).
- <sup>22</sup>P. Rosa, H. Kathrin, F. Kristian, and S. Ullrich, "Metastable underwater superhydrophobicity," *Phys. Rev. Lett.* **105**, 166104 (2010).
- <sup>23</sup>X. Zhu, R. Verzicco, X. Zhang, and D. Lohse, "Diffusive interaction of multiple surface nanobubbles: Shrinkage, growth, and coarsening," *Soft Matter* **14**, 2006 (2018).
- <sup>24</sup>S. P. Wang, Q. X. Wang, D. M. Leppinen, A. M. Zhang, and Y. L. Liu, "Acoustic bubble dynamics in a microvessel surrounded by elastic material," *Phys. Fluids* **30**, 012104 (2018).
- <sup>25</sup>P. Y. Lv, Y. L. Xiang, Y. H. Xue, L. Hao, and H. L. Duan, "Morphological bubble evolution induced by air diffusion on submerged hydrophobic structures," *Phys. Fluids* **29**, 032001 (2017).
- <sup>26</sup>S. L. Huang, P. Y. Lv, and H. L. Duan, "Morphology evolution of liquid-gas interface on submerged solid structured surfaces," *Extreme Mech. Lett.* **27**, 34 (2019).
- <sup>27</sup>H. Jari and H. Jens, "Slip flow over structured surfaces with entrapped microbubbles," *Phys. Rev. Lett.* **100**, 246001 (2008).
- <sup>28</sup>I. U. Vakarelski, J. O. Marston, D. Y. Chan, and S. T. Thoroddsen, "Drag reduction by Leidenfrost vapor layers," *Phys. Rev. Lett.* **106**, 214501 (2011).
- <sup>29</sup>L. M. Martyushev, A. I. Birzina, and A. S. Soboleva, "On the morphological instability of a bubble during inertia-controlled growth," *Physica A* **499**, 170 (2018).
- <sup>30</sup>V. Pandey, G. Biswas, and A. Dalal, "Effect of superheat and electric field on saturated film boiling," *Phys. Fluids* **28**, 052102 (2016).
- <sup>31</sup>Z. H. Wu, H. B. Chen, Y. M. Dong, H. L. Mao, J. L. Sun, S. F. Chen, V. S. J. Craig, and J. Hu, "Cleaning using nanobubbles: Defouling by electrochemical generation of bubbles," *J. Colloid Interface Sci.* **328**, 10 (2008).
- <sup>32</sup>M. S. Plesset and A. Prosperetti, "Bubble dynamics and cavitation," *Annu. Rev. Fluid Mech.* **9**, 145 (2003).